2018

Effects of porosity and contaminant on evaporation from nanopores

BOSTON UNIVERSITY

COLLEGE OF ENGINEERING

Thesis

EFFECTS OF POROSITY AND CONTAMINANT ON EVAPORATION FROM NANOPORES

by

HAOWEN CHEN

B.E., Harbin Institute of Technology, 2016

Submitted in partial fulfillment of the

requirements for the degree of

Master of Science

2018

Approved by

First Reader

Chuanhua Duan, Ph.D.
Assistant Professor of Mechanical Engineering
Assistant Professor of Materials Science and Engineering

Second Reader

Joseph Scott Bunch, Ph.D.
Associate Professor of Mechanical Engineering
Associate Professor of Materials Science and Engineering
Associate Professor of Physics

Third Reader

Tyrone Porter, Ph.D.
Associate Professor of Mechanical Engineering
Associate Professor of Materials Science and Engineering
Associate Professor of Biomedical Engineering

ACKNOWLEDGMENTS

Firstly, I want to express my gratitude to my advisor Professor Chuanhua Duan. Without his support and encouragement, I could not successfully achieve the goal. Also, I really appreciate his requirement of high academic standard which makes me learn a lot. Professor Duan is not only a great advisor, but also a great person. It's my pleasure to pursue my Master of Science degree under Professor Duan's guidance. And I believe what I have learned from him and the NEFT Lab will benefit me all through my life time.

I want to thank my thesis committee members, Prof. Scott Bunch and Prof. Tyrone Porter for their valuable advice and insightful guidance on my thesis, and their encouragement for my study. I really appreciate that they could accept my invitation to serve on my committee.

I also want to say thank you to all my Labmates whether they are here or not, including Yinxiao Li, Siyang Xiao, Zhengyu Song, Rami, Yazbeck, Mohammad, Amin Alibakhshi, Quan Xie, and Yixin Xu. When I joined NEFT Lab, I followed Yinxiao's project on evaporation from nanopore. He is the pioneer and the first person who taught me device fabrication and characterization. Also, Siyang, Rami and Mohammad offered their generous help. It is enjoyable to discuss research problem with them. I would like to thank Zhengyu for his help on experiments and thank Quan and Yixin for their help when I face research challenges.

Some of my friends, I also want to say thank you to them. Yaoye Hong, Juanyong Li, and Tianyu Jing, their suggestions help me a lot. And all my friends here today, I really enjoy the time with you guys.

All in all, I would like to express my appreciation to my parents. They are always on my back. Without their support, I could not finish my MS degree. I hope all my work will make them proud of me. I love them.

EFFECTS OF POROSITY AND CONTAMINANT ON EVAPORATION FROM NANOPORES

HAOWEN CHEN

ABSTRACT

Evaporation from nanopores, owing to its high mass/heat fluxes and high heat transfer coefficients, have found widespread applications in various industrial process, including electronics cooling, solar steam generation, membrane distillation and power generation. To further improve the performance of these nanopore-evaporation-associated processes, it is necessary to experimentally quantify the ultimate transport limit of evaporation from nanopores and understand its dependence on nanoscale confinement and operating conditions. This ultimate transport limit has now been widely accepted to be dictated by evaporation kinetics at the liquid-vapor interface, which is very difficult to quantify experimentally due to the ultra-small evaporation rates from single nanopores. To overcome this challenge, a new measurement approach based on a hybrid nanochannel-nanopore device design has been developed recently. This measurement approach can accurately measure evaporation rates/fluxes from single nanopore and has been used to investigate the effect of nanopore diameter on kinetic-limited evaporation flux. Although this study provides us new fundamental understanding about how nanoscale confinements change evaporation from nanopore, the effects of contaminant and pore porosity, which to some extent determines the practical performance of evaporation from nanopores, have remained elusive. Such lacking understanding has prevented us from developing optimized evaporative nanoporous structures for practical applications.

This works aims to investigate the effects of porosity and contaminant on kinetic-limited evaporation flux by experimentally measuring kinetic-limited evaporation rates from nanopore arrays. A modified hybrid nanochannel-nanopore device design is used to achieve this goal. In this modified device design, a nanopore array is directly connected to a 2-D nanochannel and the total evaporation rate from the nanopore array is measured by tracking meniscus receding in the nanochannel during a drying/evaporation process. Using this modified device design, we measured the kinetic-limited evaporation rates from 3x3 nanopore arrays with different interval distances ranging from 200 nm to 1 μm. To facilitate comparison between different devices, the total evaporation rates were converted to evaporation fluxes based on the nanopore projected area. Our results showed that that porosity or nanopore interval distance has negligible effect on the kinetic-limited evaporation flux. We also performed evaporation experiment using water with impurity and studied the effect of contaminant on kinetic-limit evaporation flux. It was observed that the contaminants in water can significantly reduce the kinetic-limited evaporation flux in nanopores and the contaminant effect becomes much more obvious in smaller nanopore due to contaminant-accumulation-induced pore blockage.

TABLE OF CONTENTS

LIST OF FIGURES

Chapter 1 Introduction

Evaporation from nanopores is a thin-film evaporation-based heat/mass transfer strategy. This strategy takes the advantage of large capillary force in nanopores to drive the liquid toward the nanopore entrance and maintain a steady thin liquid film around the meniscus. The presence of the steady thin film minimizes the thermal resistance between the solid substrate and the liquid/vapor interface, allowing fast evaporation below the liquid saturation temperature. Consequently, high heat/mass flux and large heat transfer coefficients can be simultaneously achieved (Plawsky et al., 2014).

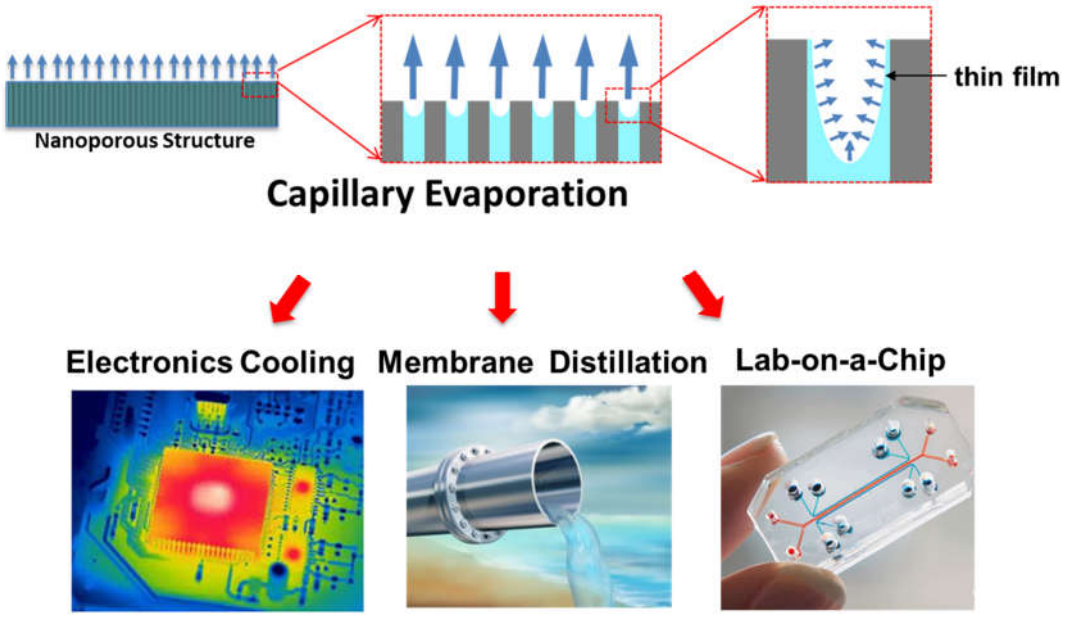

Figure 1.1 Application of evaporation from nanopores in different areas (Li, 2017)

Because of the efficient heat/mass transfer, evaporation from nanopores has been employed in a variety of industrial applications. For example, because of its capability of removing high heat fluxes while maintaining relatively low operating temperatures in limited spaces,

evaporation from nanopores provides a new paradigm for thermal management of high-power electronics and weapons. Heat fluxes needed to be dissipated from these devices are reaching several hundreds or even one thousand Watts per square centimeter, which cannot be efficiently removed by traditional thermal solutions (Bowers et al., 1994; Lu et al., 2017; Lu et al., 2016; Narayanan et al., 2013; Vafai et al., 1999; Xiao et al., 2013). Evaporation from nanopore have also be used in membrane-based distillation and purification (Alkhudhiri et al., 2012; Khayet, 2011; Lee & Karnik, 2010), solar vapor generation(Fang et al., 2017; Ghasemi et al., 2014), and power generation(Wang & Chen, 2018). In addition to these industrial applications, it has been observed that evaporation from nanopore is critical for several natural processes such as plan transpiration and mammalian perspiration (Buckley et al., 2017; Rand, 1983).

Despite its important implication, our understanding of this nanoscale phase change phenomenon is far from complete. To date, there have only been limited theoretical and experimental studies focusing on exploring fundamental mechanisms of evaporation from nanopores. Although these studies to a large extent showed that the classical evaporation theory, derived based on quasi-equilibrium evaporation conditions, cannot accurately describe evaporation from nanopores, they have not provided yet complete explanations why the classical theory fails and how intense evaporation under non-equilibrium conditions and nano confinements would affect evaporation from nanopores. What's more, effects of contaminant and pore porosity, which to some extent determine the practical performance of evaporation from nanopores, have not been studied. Such lacking

understanding has prevented us from further understanding those related natural processes and developing new evaporative structures with better performance for existing and new applications.

This work aims to experimentally investigate evaporation from nanopores and to further understand the effects of confinement, porosity and contaminant on the evaporation flux. In the following parts of this chapter, we will first give a brief introduction to the classical evaporation theory and explain why it may not be valid at the nanoscale. This will be followed by a summary of recent theoretical and experimental studies of evaporation from nanopores. Finally, the motivation and scope of this work will be presented.

1.1 Fundamental mechanism of evaporation from nanopores

Figure. 1.2 shows the schematic diagram of evaporation from a nanopore. It is evident that this phase change phenomenon consists of three different mass transport processes: (a) liquid transport to the nanoscale liquid-vapor interface; (b) liquid vaporization at the nanoscale liquid-vapor interface; and (c) removal of generated vapor by diffusion and advection (Plawsky et al., 2014).

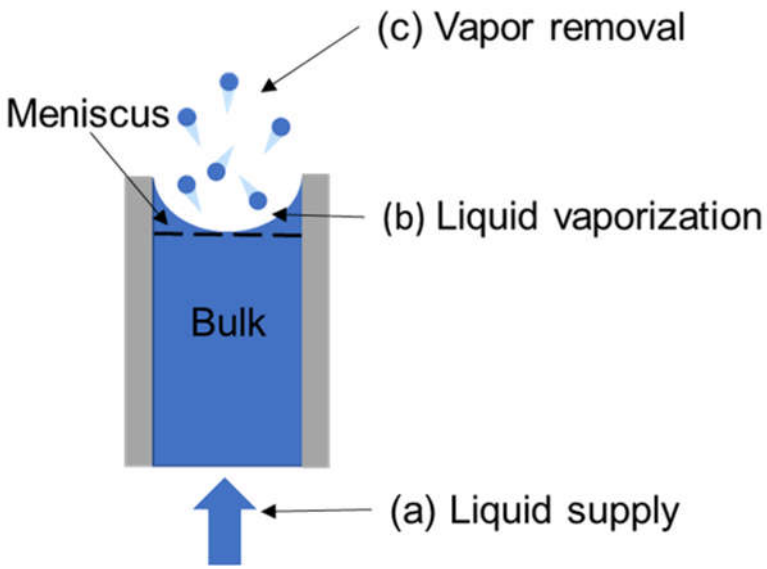

Figure 1.1 Schematic of evaporation from nanopore

Among all the three processes, the liquid transport and vapor removal process have been well studied and can be easily controlled by changing the device structure and experiment conditions. Compare with these two transport processes, the liquid vaporization process at the nanoscale liquid-vapor interface, governed by the local evaporation/condensation kinetics, is much less understood. This process is thus the most difficult process to control and becomes the ultimate limiting process for evaporation from nanopore. The corresponding evaporation fluxes/rates are typically referred to as the kinetic-limited evaporation fluxes/rates.

There are many challenges in quantifying the kinetic-limited evaporation fluxes/rates in nanopores. Traditionally, according to the classical kinetic theory (CKT), the local kinetic-

limited evaporation flux can be calculated using the Hertz-Knudsen relation (Hertz, 1882; Knudsen, 1950):

$$m_k'' = \sqrt[2]{\frac{M}{2\pi R}}\left(\sigma_e \frac{P_{V,eq}}{\sqrt{T_{li}}} - \sigma_v \frac{P_v}{\sqrt{T_v}}\right) \tag{1.1}$$

where M is the molar mass, R is the constant gas number, σ_e and σ_c is the evaporation and condensation coefficient, $P_{v,eq}$ is the equilibrium pressure right over the liquid interface, P_v is the vapor pressure, T_{li} and T_v is the liquid and vapor temperature. Although this expression has been proposed for more than a century, it is very challenging to use it to accurately calculate the local evaporation flux even for a flat liquid-vapor interface. The reason behind this is because the H-K equation was derived based on an assumption of quasi-equilibrium evaporation conditions. The validity of this equation under intense non-equilibrium evaporation conditions has been questioned. What's more, even if this expression is still valid, the values of both two empirical coefficients, evaporation coefficient σ_e and condensation coefficient σ_c are under debate. Different values ranging from 10^{-3} to 1 have been reported over the last century (Marek & Straub, 2001).

In addition to these two issues regarding quantification of the local evaporation flux, the nanoscale confinements of the nanopores also make accurate prediction of kinetic-limited evaporation fluxes/rates from nanopore difficult. First of all, it is very difficult to quantify the actual evaporation area for an evaporation meniscus in a nanopore due to strong surface-liquid interactions. Secondly, it is unclear if evaporation from the highly curved menisci will be the same as evaporation from flat liquid-vapor interface. Last but not the

least, the nanoscale confinements may also change the interfacial water structure and thus further change the evaporation coefficient.

Because of all these challenges listed above, a quantitative and systematic understanding of kinetic limited evaporation in nanopores have not been achieved.

1.2 Recent theoretical and experimental studies

Realizing the problems of traditional HK equation, researchers have recently developed several theoretical models based on CKT to predict the kinetic-limited evaporation flux in nanopores(Lu et al., 2015; Narayanan et al., 2011; Pati et al., 2013). Still there are many conflicts between different models. For example, Narayanan (2011) developed a semi-analytical, continuum model to study kinetic-limited evaporation from 1D cylindrical nanopores. This model used the Navier-Stokes equation to describe liquid water transport towards the meniscus and used the augmented Young-Laplace equation (considering surface-liquid interactions and disjoining pressure) to characterize the meniscus. They concluded that the solid-liquid interactions would extend the evaporation meniscus as the radius of pore decreases which would greatly enhance the effective evaporation flux (i.e., evaporation rate per project pore area). Different from this study, Lu (2015) developed another model based on ballistic transport and radiation analogy to study the evaporation from 1D cylindrical nanopores. However, they found that the kinetic-limited evaporation flux of nanopore would not change with the radius of pore.

Because of the inconsistence between CKT-based models, recently a new theoretical approach based on Statistical Rate Theory (SRT) has been proposed. The SRT approach was originally developed to describe the rate of particle transport across a phase boundary using the concept of transition probabilities between quantum states(Ward & Fang, 1999). Ward et al. (1999) started using this approach to describe evaporation kinetic at the liquid-vapor interface. In a recent paper written by Persad and Ward (2016), they conducted a thorough examination of existing theoretical, experimental, and molecular dynamics (MD) simulation studies of evaporation kinetics and derived the expression for the kinetic-limited evaporation flux based on the SRT approach. By comparing the measured vapor pressure P_v and the calculated vapor pressure P_v^* (using the SRT theory), they concluded that that the SRT theory can properly grasp the physical mechanism of evaporation. Although this SRT theory seems to be able to explain a variety of existing evaporation results at the macro/microscale, it is not clear if this theory could also successfully describe evaporation kinetics and evaporation coefficients in nanoscale confined spaces where the liquid structure may be significantly different from the bulk liquid. Consequently, a quantitative understanding of evaporation kinetics in nanoscale confinements has not yet achieved.

Because of all the challenges for theoretical study, experimental study becomes an alternative to study the kinetic-limited evaporation from nanopores. The first challenge of the experimental study is to find a method that can accurately measure the kinetic-limited evaporation flux. Most current experimental studies solved this challenge by directly measuring evaporation from existing nonporous membranes (Dai, Famouri, et al., 2013;

Dai, Huang, et al., 2013; Dai, Yang, et al., 2013; Lu et al., 2016; Narayanan et al., 2013; Xiao et al., 2013; Yang et al., 2018). Although these studies did observe relatively high evaporation performance, they cannot provide much insight about the kinetic-limited vaporization process at the nanoscale liquid-vapor interface because evaporation in these membranes are either limited by the liquid water transport towards the interface or vapor removal from the interface. Meanwhile, because of the pore polydispersity of existing nanoporous membranes, it is very difficult to quantify the evaporation flux for single nanopores and investigate the effect nanoscale confinement on evaporation flux.

To solve these problems, Li et al. (2017) developed a new evaporation measurement approach based on a hybrid nanochannel-nanopore device design. This approach enables direct measurement of the evaporation rates/fluxes from single nanopores while guaranteeing the sufficient water supply and high vapor removal efficiency. Li et al. (2017) used this approach to measure kinetic-limited evaporation from single nanopore with diameter ranging from 27 to 225 nm. Their results showed that the kinetic-limited evaporation flux increases with the decreasing nanopore diameter, which can be one order of magnitude higher than the maximum theoretical predication based on the classical Hertz-Knudsen relation

Although Li et al.'s study (2017) has provided us new fundamental understanding how nanoscale confinements change evaporation from nanopore, the effects of contaminant and pore porosity on the kinetic-limited evaporation from nanopore, which to some extent

determines the practical performance of evaporation from nanopores, have not been experimental investigated. Quantifying and elucidating these two effects would help develop optimized evaporative nanoporous structures for practical applications.

1.3 Motivation and scope of study

This thesis aims to measure and understand the effects of porosity and contaminant on kinetic-limited evaporation rates/fluxes in nanopore arrays using a modified hybrid-nanochannel-nanopore device design. In chapter 2, the nanofluidic device-based evaporation measurement technique is introduced first. This is followed by a detailed description of fabricating and characterizing the modified hybrid nanochannel-nanopore devices. Methods of changing the porosity of the nanopore array and changing contaminant concentration is also discussed in this chapter. In chapter 3, experimental results of the kinetic-limited evaporation flux in nanopores as a function of porosity (interval distance) and contaminant concentration are presented and discussed. A brief discussion of future work is also provided at the end of this chapter.

Chapter 2 Experiment

2.1 Design of Hybrid nanochannel-nanopore device

The essential idea of measuring evaporation rates/fluxes in nanopores using the hybrid nanochannel-nanopore device is mass conservation and capillary pressure difference. Figure. 2.1 shows the schematic of a hybrid nanochannel-nanopore device. When a water-filled hybrid nanochannel-nanopore devices starts drying, two menisci will form at the entrances of the nanopore and the nanochannel, respectively. Because of the feature size difference between the long reference nanochannel and short nanopore, the capillary pressure in the nanopore is much larger than the capillary pressure in the nanochannel. When liquid starts evaporating from the nanopore, the capillary pressure difference will force the meniscus in the nanopore to be pinned at the top entrance of the nanopore. Meanwhile, the meniscus in the nanochannel will be pushed to recede towards the nanopore. The capillary pressure difference between the nanochannel and the nanopore is expressed as equation (2.1):

$$\Delta P = \frac{4\sigma cos\theta}{d} - \frac{2\sigma cos\theta}{h} \tag{2.1}$$

where σ is the surface tension of water, θ is the contact angle of water, d is the diameter of nanopore, and h is the height of nanochannel.By recording the receding speed of the meniscus in the nanochannel and using mass conservation, the kinetic-limited evaporation flux can be calculated using equation (2.2), when the water drying process in nanochannel is negligible.

$$V = \frac{V_{ref}Wh}{\frac{1}{4}\pi d^2} \tag{2.2}$$

In this equation, V is the kinitic-limited evaporation flux of the nanopore, V_{ref} is the velocity of receding meniscus in the nanochannle, W is the width of the nanochannel, h is the height of the nanochannel, d is the diameter of the nanopore.

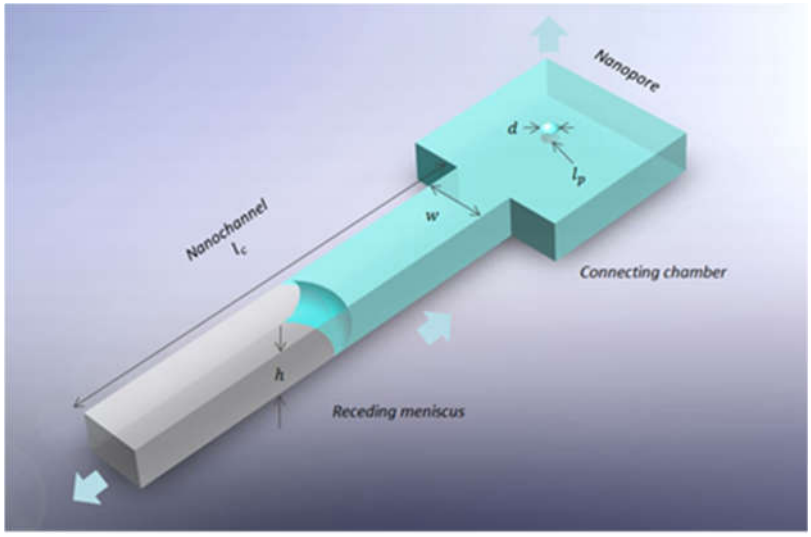

Figure 2.1 Schematic of hybrid nanochannel-nanopore device (Li 2017)

2.2 Fabrication and characterization of hybrid device

Fig. 2.2 shows the fabrication process of the hybrid nanochannel-nanopore device. The fabrication process consists of two parts, i.e., fabrication of the nanopore component and fabrication of nanochannel/microchannel component. Fabrication of the nanopore component starts with a 4" silica wafer. As the first step, 200 nm low-pressure chemical vapor deposition (LPCVD) silicon nitride was deposited on both sides of the wafer (LPCVD, see Figure. 2.2a). Then photolithograph and reactive ion etching (RIE) were used to open window on one side of silicon nitride. After that, 30% KOH solution was used to do anisotropic etching. As shown in Figure. 2.2b, after the KOH etching, suspended silicon

nitride membrane was formed. Finally, focus ion beam (FEI Quanta 3D FEG FIB) with 10PA aperture was used to create nanopores on the suspended membrane (Figure. 2.2c).

Different from the nanopore component, fabrication of the nanochannel component start from a 4" glass wafer. First of all, the nanochannels and microchannels were patterned on a separate glass wafer by using the photolithography and RIE. As shown in Figure. 2.2d-f, nanochannels were firstly created on the glass wafer using photolithography and RIE. Then, by using aligned lithography, the nanochannels were carefully covered by photoresist and the microchannels used for water introduction to the nanochannels were defined. RIE was used again to etch the microchannels. After finishing fabrication of nanochannels and microchannels, the glass wafer was cut into individual chips by dicing saw. The nanochannel and the nanopore chips were then cleaned in Piranha solution (98% H2SO4: 30% H2O2 = 3:1) for 5 mins, after which they were aligned under a microscope and subsequently bonded together using a home-made anodic bonding setup at 800V and 400 ºC. After bonding, the devices were put in oxygen plasma chamber to clean for 10 mins.

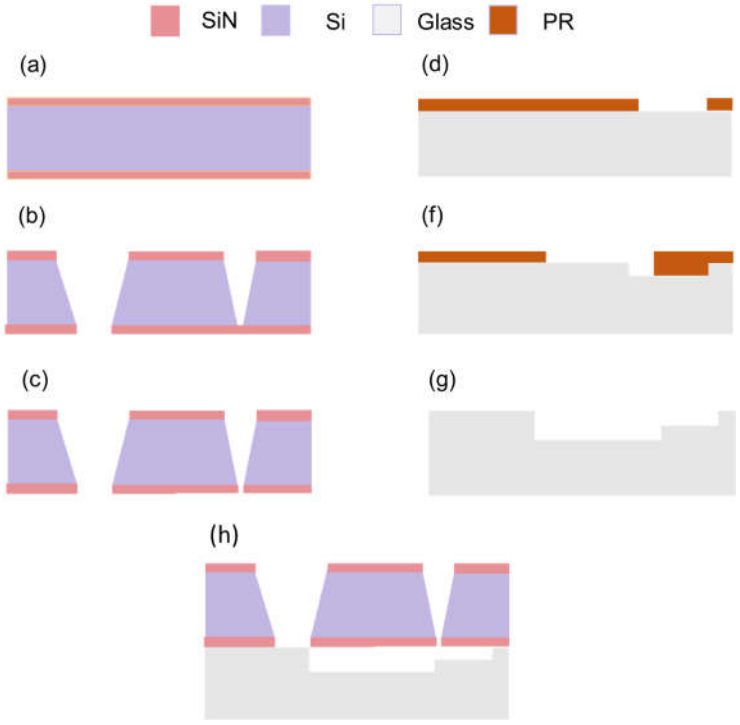

Figure 2.2 Fabrication process of nanochannel-nanopore device hybrid

To use the hybrid nanochannel-nanopore device to accurately quantify evaporation rates/fluxes in nanopore, it is very important to characterize the device and measures the dimensions of the nanochannels and nanopores. Fig. 2.3 shows the microscopic image (Fig. 2.3a&b) of a well bonded nanochannel-nanopore device and the corresponding nanochannel (AFM image, Fig. 2.3c&d). Each device only includes one hybrid nanochannel-nanopore. However, a series of nanochannel and connecting chamber were designed and fabricated to facilitate the alignment process before anodic bonding. The nanochannel height was carefully measured by AFM, Figure 2.3 c&d shows a three dimensional and cross-sectional image of a 150 nm nanochannel.

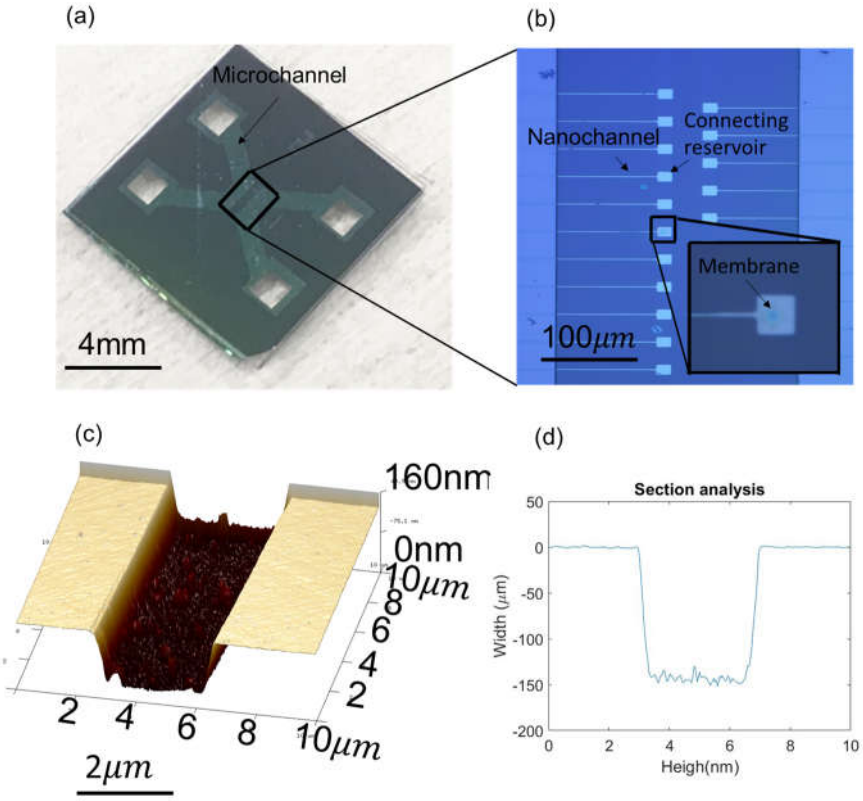

Figure. 2.3 Hybrid nanochannel-nanopore device. (a&b) optical microscopic image of a hybrid device. (c&d) AFM image of 150 nm high nanochannel.

The nanpores in the hybrid device were characterized using scanning electron microscope (SEM). As shown in Figure. 2.4, a 3×3 nanopore array is milled on 200 nm silicon nitride membrane. To study the porosity effects, it's important to fabricate suitable number of nanopores on the membrane. When the number of the nanopores is too large, even though it may beeasier to observe the porosity effect, the menicus receeding speed in nanochannel is too fast to record. When the number of nanopores is too small, comparing to the drying process in nanochannel, it will be hard to extract the contribution of evaporation from nanopores. We found that the 3x3 nanopore array is a good configuration for both experimental measurements and porosity investigation. By using the 3×3 nanopore array,

for each single nanopore, there are at least other three nanopores adjacent to it and consequenlty the porosity effect, a.k.a., the effect of evaporation from surrounding nanopores, should be evident.. Meanwhile, the total evaporation rates (liquid water loss) from these nine nanopores are found to be larger than water drying from the nanochanel and we can easily calculate the evaporation flux/rate from the raw experimental data.

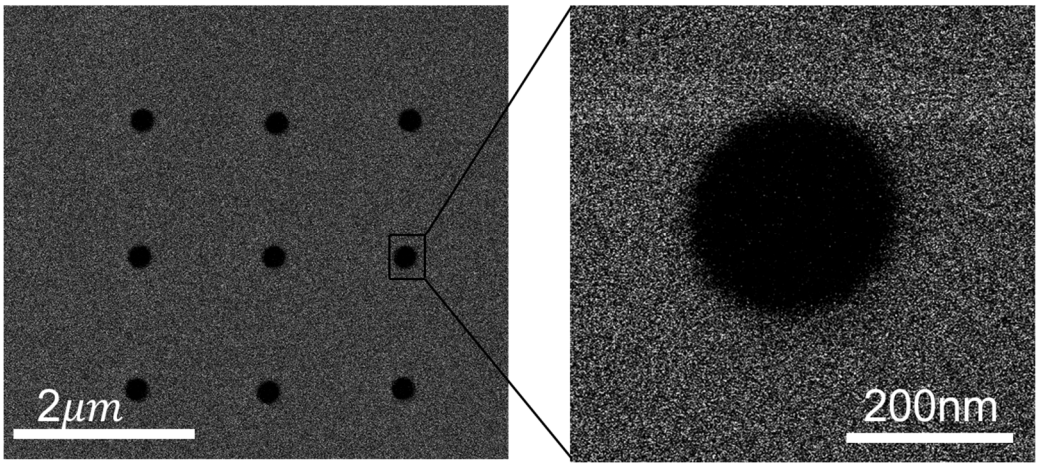

Figure 2.4 SEM image of nanopores on a membrane milled by FIB. (a) nine identical pores are milled on membrane, interval distance is 1.5μm. (b) A typical milled nanopore with a diameter of 231±5 nm.

In this work, 7 hybrid nanochannel-nanopore devices were fabricated and tested., The corresponding pore diameter d and channel height h, expressed as $\frac{d}{h}$, are, $\frac{92\pm5nm}{200\ nm}$, $\frac{95\pm5\ nm}{203\ nm}$, $\frac{124\pm5nm}{233\ nm}$, $\frac{122\pm5nm}{233\ nm}$, $\frac{100\pm5nm}{206\ nm}$, $\frac{235\pm5nm}{206\ nm}$, $\frac{242\pm5nm}{206\ nm}$, respectively.

2.3 Measurement and data analysis

Fig. 2. 5 shows the experimental setup. The hybrid device is placed inside a vacuum chamber and the ambient temperature was 20 ºC. To record the location of the meniscus in the nanochannel, an inverted microscope (Olympus IX81 ZDC) was placed at the bottom of the vacuum chamber. To begin with the experiment, the deionized water was introduced into device through the big reservoir and microchannels. Water would immediately fill the microchannel, nanochannel and connecting reservoir with nanopores on it.

Once the water filled all the connecting reservoir and the nanochannels, a mechanical pump was used to reduce the pressure in the vacuum chamber to 150Pa and initialize the evaporation process. It would usually take 2-5 minutes to dry the water in the big reservoirs and the microchannels. Because of the capillary pressure difference, when evaporation started, only the meniscus in nanochannel would start to recede. The location of receding meniscus was recorded by a high-speed camera (Hamamatsu ORCA-Flash4.0: 100 fps with 512 pixels × 512 pixels).

To investigate the effects of contaminant, HCl solutions at different concentrations were used as the working fluids. HCl solution is used as it has been reported protons could change interfacial water structure and thus affect evaporation kinetics. For example, for a micro scale HCl droplet, it's reported that the hydronium at liquid/vapor interface is indeed preferentially adsorbed which causes the pinning of instantaneous surface height fluctuations of water(Otten et al., 2012; Rizzuto et al., 2017). Because more water molecular was pinned by hydronium

at liquid/vapor interface, the evaporation rate is reduced. To prepare these solutions, 37% HCl was firstly diluted in deionized water using different dilution ratios. After the preparation of different concentration HCl solution, the conductivity of each HCl solution was measured by a pH meter (Sevencompact^{TM} S230). By using the conductivity of HCl solution, we can directly calculate the pH of HCl solution. The prepared HCl solution were introduced in the hybrid nanochannel-nanopore device for nanopore evaporation experiments in either ascending or descending order of pH. To ensure that the surface properties of nanopores remain the same between different experiments. Meanwhile, to avoid the effects of concentration gradient, 10min oxygen plasma cleaning is conducted after each evaporation experiment.

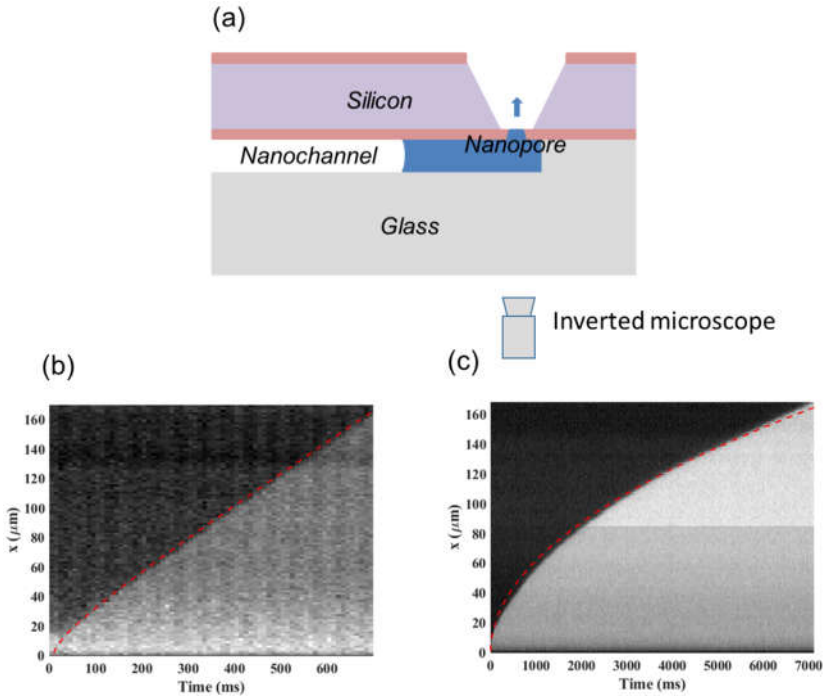

Figure. 2.5 (a) schematic of experiment setup (b) Tracking curve of meniscus location in nanochannel as function of time (d = 124±5 nm) (c) Tracking curve of meniscus location in nanochannel as function of time with PDMS blockage

Fig. 2.5b shows a typical tracking curve of the meniscus location in the nanochannel as function of time during a nanopore evaporation experiment. Because evaporation from nanopores and water drying in the corresponding nanochannel would both contribute to meniscus receding in the nanochannel, the meniscus receding speed in the nanochannel measured from the experiment cannot be directly substituted in equation (2.1) to calculate the kinetic-limited evaporation flux from the nanopores. In fact, considering the two major contributions to the meniscus receding, the meniscus receding process can be described by the equation (2.3) listed below:

$$\frac{dx}{dt} = D\frac{\rho_{v,n}-\rho_{v,e}}{x\rho_l} + V_{ref} \tag{2.3}$$

where D is the equivalent diffusion coefficient of water vapor, and $\rho_{v,n}$ is the saturated vapor density at the receding meniscus interface and $\rho_{v,e}$ is the vapor density of outside the nanochannel, p_l is the liquid density, and V_{ref} is the meniscus receding speed in the nanochannel caused by to nanopore evaporation.

In equation (2.3), if we want to get the $V_{ref,\text{ the}}$ equivalent diffusion coefficient D should be quantified in advance. So, in a separate experiment, a PDMS block was placed on the top of nanopore window to prevent evaporation from nanopore and the position of meniscus in the nanochannel was recorded again (see Fig. 2.5c). Because of the elimination of evaporation, the meniscus receding process in nanochannels would be only governed by drying along the nanochannel, which can be described as equation (2.4):

$$\frac{dx}{dt} = D\frac{\rho_{v,n}-\rho_{v,e}}{x\rho_l} \tag{2.4}$$

By integrating of equation (2.4), we can get equation (2.5):

$$x = \sqrt{2D\frac{(\rho_{v,n}-\rho_{v,e})t}{\rho_l}} + C_1 \tag{2.5}$$

By fitting the meniscus tracking curve in Fig. 2.5c with equation (2.5), the equivalent diffusion coefficient *D* could be calculated. In Fig 2.5c, the equivalent diffusion coefficient is 1.1 cm^2/s.

By substituting the equivalent diffusion coefficient D in equation (2.3) and subsequently solving this equation, we could correlate the meniscus location and time using equation (2.6):

$$t = \frac{x}{V_{ref}} - D\frac{(\rho_{v,n}-\rho_{v,e})}{\rho_l V_{ref}^2} ln\left\{\frac{(\rho_{v,n}-\rho_{v,e})}{\rho_l} + xV_{ref}\right\} + C_2 \tag{2.6}$$

Using data fitting again, the meniscus receding speed V_{ref} due to evaporation from the nanopores can then be easily extracted. Finally, the evaporation flux from a single nanopore can be calculated as $\dot{Q} = \frac{4V_r wh}{N\pi d^2}$, where N is the number of nanopores in the membrane

Chapter 3 Result and analysis

3.1 Effects of porosity

For nanopore array, since the porosity is essentially determined by the interval distance between each single pore, to study the effects of porosity on kinetic-limited evaporation, the interval distance between each single pore should be the only one independent variable in the experiment. To achieve this goal, we have to control all the other variables to eliminate their potential effects on kinetic-limited evaporation.

Based on our previous studies and the classic evaporation kinetics theory, we have learned that the kinetic-limited evaporation flux in nanopores strongly depends on the operating temperature, vapor pressure and nanopore diameter. Consequently, all these three variables should be well controlled to enable comparison between different nanopore arrays. In this work, we kept the operating temperature at 20 °C and used a vacuum pump to control the pressure to be 150 Pa.

Although we were able to control the operating temperature and pressure of, we had great difficulty in creating 3x3 nanopore arrays with similar nanopore diameters but different interval differences using FIB. We were only able to get two sets of nanopore arrays and each set only include two nanopore arrays with different interval distances. The diameters (d) and interval distances (l) for the first set of the nanopore arrays, written in the form of $\frac{92\pm5nm}{454nm}$ and $\frac{92\pm5nm}{940nm}$, respectively. In contrast, the diameters (d) and interval distances (l) for the second set of the nanopore arrays, are $\frac{122\pm5nm}{200\,nm}$ and $\frac{124\pm5nm}{543nm}$ respectively.

The error bars for the diameter correspond to the measurement uncertainty in the SEM characterization, which is ±5 nm. The error bars for the evaporation flux correspond to the uncertainties of pore diameter characterization, nanochannel height/width characterization and meniscus receding speed estimation.

Figure 3.1 plots the evaporation fluxes of these two sets of nanopore array measured using the hybrid nanochannel-nanopore devices. The error bars for the diameter correspond to the measurement uncertainty in the SEM characterization, which is ±5 nm. The error bars for the evaporation flux correspond to the uncertainties of pore diameter characterization, nanochannel height/width characterization and meniscus receding speed estimation.

For the first set, as we can see from Figure. 3.1, the measured kinetic-limited evaporation flux for the nanopore array with a diameter of 92±5 nm nanopores and an interval distance of 454 nm, is 2.69 mm/s and the corresponding errors (mainly induced by diameter measurement uncertainty are +0.32 mm/s, -0.27 mm/s, respectively. For the nanopore array with a diameter of 92±5 nm nanopores and an interval distance of 940 nm, the measured kinetic-limited evaporation flux is 2.99 mm/s and the corresponding errors of kinetic limited evaporation flux caused by diameter correcting is are +0.35 mm/s, -0.30 mm/s, respectively. Therefore, if we consider all measurement uncertainties, errors induced by the nanopore diameter, the actual kinetic-limited evaporation flux for the nanopore array with of 454 nm interval distance is at the range from between 2.42 mm/s (2.69 – 0.27 = 2.42 mm/s) and to 3.01mm/s (2.69 + 0.32 = 3.01 mm/s), and the actual kinetic-limited

evaporation flux for the nanopore array with an interval distance of 454 nm of 940 nm interval distance pores is at the range from between 2.69 mm/s (2.99 – 0.3 = 2.69 mm/s) and to 3.34mm/s (2.99 + 0.35 = 3.34 mm/s). Because the ranges of these two-actual kinetic-limited evaporation flux overlap, we can find that the two markers in Figure. 3.1 which represent the kinetic-limited evaporation flux overlap. Significantly, it is safe to say that when for the interval distance ranging from 454 nm to 940 nm, the effects of nanopore interval distance is negligible.

For the second set, the kinetic-limited evaporation fluxes for the two nanopore arrays (are $1.61\frac{+0.14}{-0.12}$ mm/s and are 1.49 $\frac{+0.13}{-0.11}$ mm/s, respectively. There is again large overlap between the ranges of the actual kinetic-limited evaporation fluxes, which suggests that the nanopore interval distance still does not influence the kinetic-limited evaporation flux, when the interval distance changes from 543 nm to 200 nm.

By combing the result of both two experiments together, the conclusion of porosity study is that when the interval distance of nanopores ranging from 200 nm to 1 μm, the effects of interval distance is negligible. In other words, the evaporation flux/rate in a certain nanopore is not affected by evaporation from surrounding nanopores and thus we can estimate the effective evaporation flux for a nanopore array by simply using the product of the evaporation flux of a single pore and the porosity.

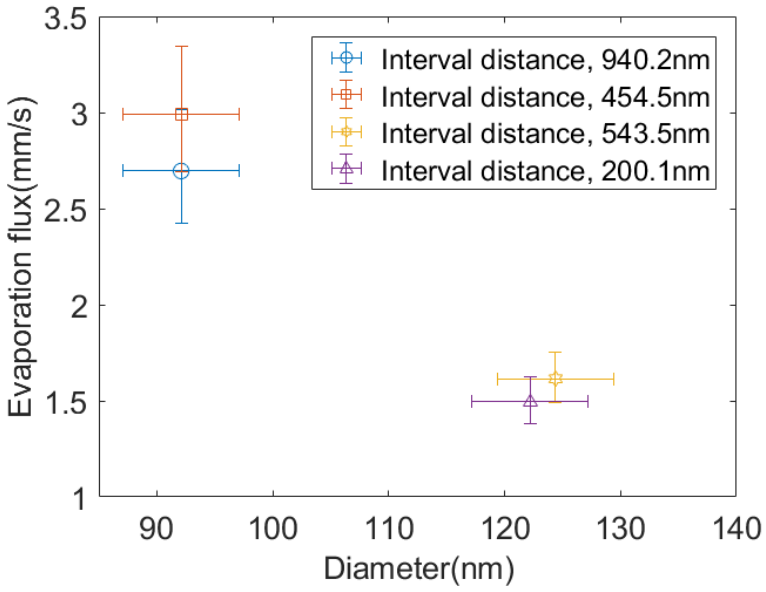

Figure. 3.1 Comparison of evaporation flux between different interval distances at the same diameter

Although there is no obvious dependence on the interval distance, it is worth noting that the measured evaporation fluxes for the first set is significantly higher than those for the second set. We believe this difference results from the different nanopore diameters of these two sets, which can significantly affect the kinetic-limited evaporation fluxes in nanopores based on Li et al.'s study. Figure 3.2 shows our result as well as Li et al.'s results measured from single or a small array of nanopores with interval distances larger than 1 μm. The consistency between these two sets of results not only confirms the dependence of the evaporation flux on nanopore dimeter, but also further confirms that the independence of the evaporation flux on the interval distance.

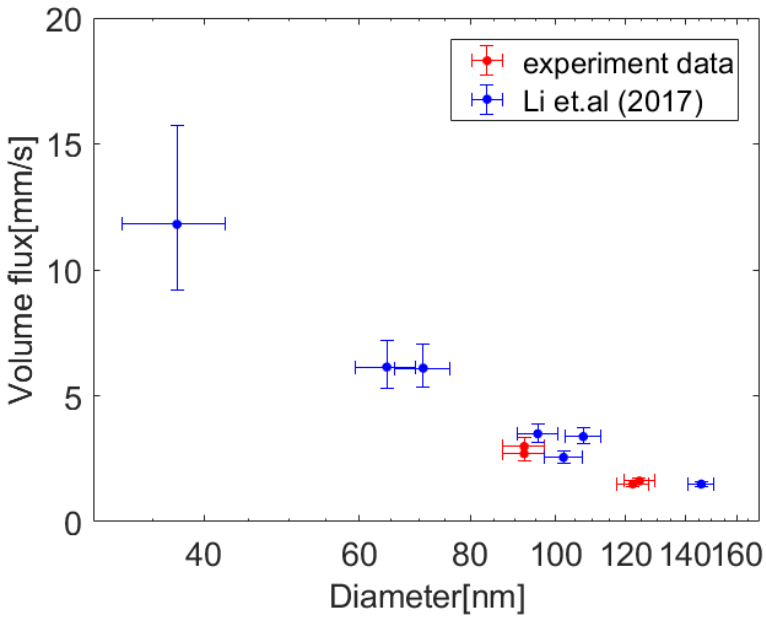

Figure. 3.2 Comparison of kinetic-limited evaporation flux between experiment data and Li et.al's data (2017)

3.2 Contaminant

It's reported that when evaporation happens at millimeter size confinement space, the liquid-vapor interface is sensitive to active containment in fluid including fatty acids, alcohols, and surface-active ions. The evaporation rate, even the evaporation coefficient will be hugely reduced (Drisdell et al., 2010; Marek & Straub, 2001; Otten et al., 2012). This contaminant reduction effect is also observed at microscale droplet, where the 1M HCl solution will decrease the evaporation coefficient(Rizzuto et al., 2017). However, for microscale droplets, despite the contaminant reduction effect, it's also reported that the 0.1molar HCl solution will increase the evaporation coefficient. Because of the two-opposite phenomena observed at microscale droplet, so we wonder, whether the kinetic-limited evaporation will be enhanced or not if HCl solutions instead of pure water

evaporate from the nanopores. To investigate the effects of HCl solution on kinetic-limited evaporation, the hybrid device (Chip.1) with 3×3 nanopore array was fabricated for which the nanopore diameter is 241 nm. DI water (pH = 7) and five different concentration HCl solution (pH = 3.99, 3.08, 2.44, 1.32, 0.08) was used as working fluid. The experiment firstly began with DI water and then was continued in pH descending order. The evaporation flux as function of fluid pH is presented by blue square marker in Figure. 3.3 which suggests that the kinetic-limited evaporation flux decreases as the fluid pH decreases. Although a decreasing trend of kinetic-limited evaporation flux was observed, since there might be some other contaminants, for example other unknown contaminants in fluid, influencing the kinetic-limited evaporation, we can't directly conclude that the decreasing trend of kinetic-limited evaporation flux corresponds only to the variation of HCl concentration. Further experiments are required to determine whether the decrease of kinetic limited evaporation flux is caused by HCl solution or not. So, for the same device Chip.1, the experiment was done again at pH ascending order (beginning with pH = 0.008). The evaporation flux as function of fluid pH is presented by orange diamond marker in Figure. 3.3.

If kinetic-limited evaporation corresponds only to the HCl solution, it's expected that, at the same pH HCl solution, no matter what the experiment order is, the kinetic-limited evaporation flux should be similar. We can find from Figure. 3.1 that when pH is ranging from 0 to 3, the kinetic-limited evaporation flux measured from the pH ascending order experiment is identical to the kinetic-limited evaporation flux measured from pH

descending order experiment. It seems that experiment result at certain pH range proves our expectation. However, still we can't directly make conclusion, because when pH = 7 (DI water), the kinetic-limited evaporation flux measured at pH ascending order is much smaller than the kinetic-limited evaporation flux measured at pH descending order, which means that not only HCl solution, but other unknown factors influence the kinetic-limited evaporation. Further experiment is required.

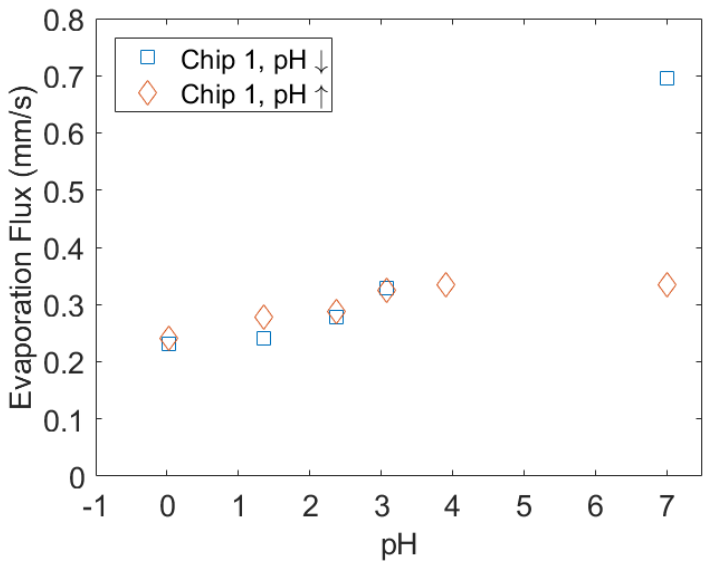

Figure. 3.3 Evaporation flux as function of fluid pH (pore diameter: 241±5nm), pH ↓ means the experiment begins with DI water, then different HCl solutions are used to do experiment at pH descending order, pH ↑ means after finishing the experiment in pH ↓ order, the experiment is continuously done at pH ascending order, begins with pH = 0.08 HCl solution,

Another chip (Chip.2) with similar nanopore diameter, was fabricated. For Chip.2, the experiment process is similar to the experiment process of Chip.1. The experiment was done firstly in pH descending order and then pH ascending order. The only difference between the Chip.1 experiment and the Chip.2 experiment is that the pH of working fluid in Chip. 2 experiments ranges from 3 to 7 (DI water, pH = 6.36, 5.65, 4.72, 3.99, 3.08 HCl solution). The evaporation flux measured from different device at different experiment order is presented as function of fluid pH in Figure. 3.3. It's clear to see that for Chip. 2, when the experiment was done in pH descending order (presented by purple circle marker), the kinetic-limited evaporation flux decrease as pH decrease. when the experiment was done in pH ascending order (presented by purple circle marker), although pH is changing from 3 to 7, the kinetic-limited evaporation flux doesn't change as the pH change. Moreover, if we are going to compare the kinetic-limited evaporation flux between Chip.1 experiment and Chip.2 experiment, we can see that the kinetic-limited evaporation flux of Chip2 is much smaller than the kinetic-limited evaporation flux of Chip.1. So, to find what caused inconsistence between Chip.1 and Chip.2, SEM image was done for both chip. As we can see from Figure .3.4 (b&c), one of the nanopore is blocked in Chip.2. It's believed that the HCl solution will not block the nanopore, there must be some other contaminant in fluid make the blockage happens. Also because of the observed blockage, when the experiment was done at ascending order, the kinetic-limited evaporation flux remains constant which is not reliable. It's also important for us to figure out when the blockage influence the kinetic-limited evaporation and if there is really a pH dependence.

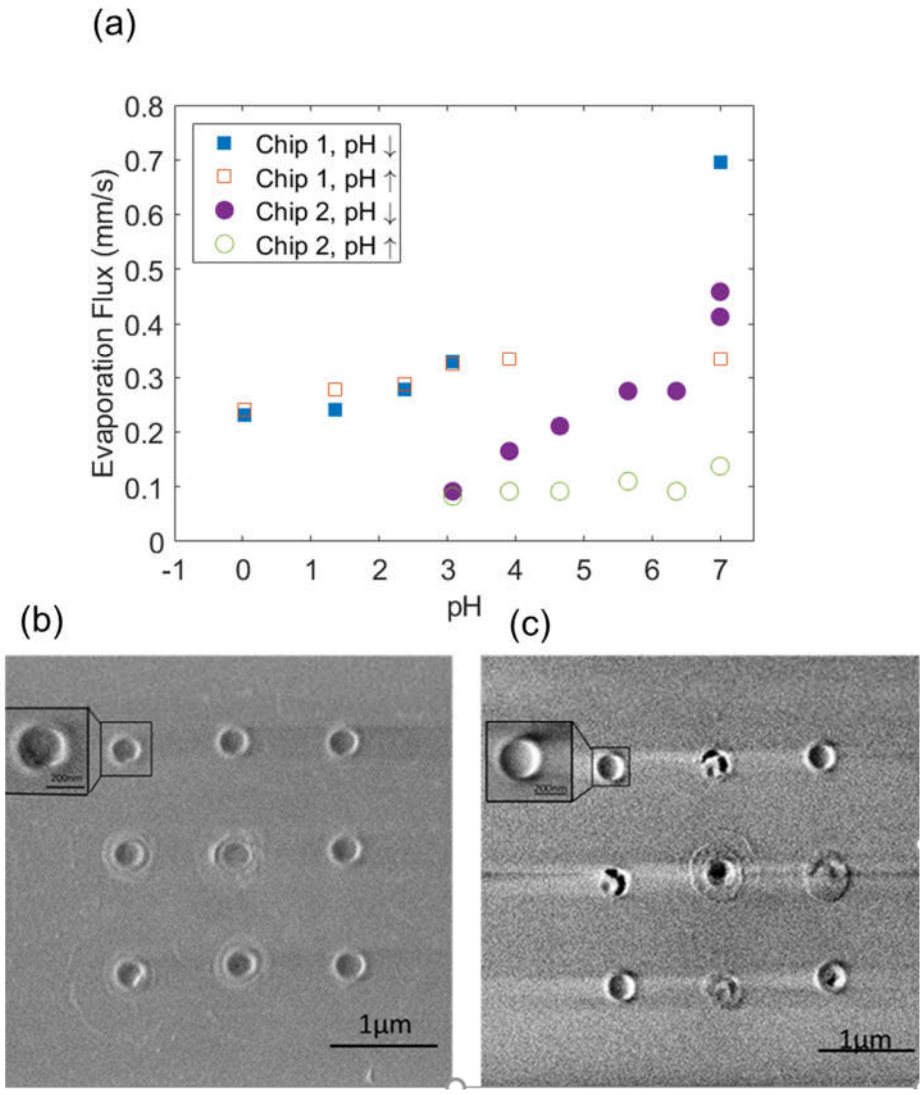

Figure. 3.4 (a) Comparison of evaporation flux as function of fluid pH between two chips (Chip.1 pore diameter: 241±5 nm, Chip.2 pore diameter: 236±5 nm), pH ↓ means the experiment begins with DI water, then different HCl solutions are used to do experiment at pH descending order, pH ↑ means after finish the experiment in pH ↓ ,the experiment is continuously done at pH ascending

order, begins with pH = 0.08 HCl solution, (b) SEM image of Chip. 1, nanopore diameter is 241±5 nm, (c) SEM image of Chip. 2, nanopore diameter is 236±5 nm

Another device, except Chip.1 and Chip.2 is used for figuring out when the nanopore blockage influence the experiment and which data point is reliable. At this time, the experiment is only done at pH descending order and it's important to note that after every working fluid is used to do the experiment, the device is rinsed by water for two minutes. Then a DI water is used to do the control experiment. As we can see from Figure. 3.5, at every pH, the kinetic-limited evaporation flux of experiment group is similar to the kinetic-limited evaporation flux of DI water control group which means that the contaminant in fluid not HCl reduce the kinetic-limited evaporation.

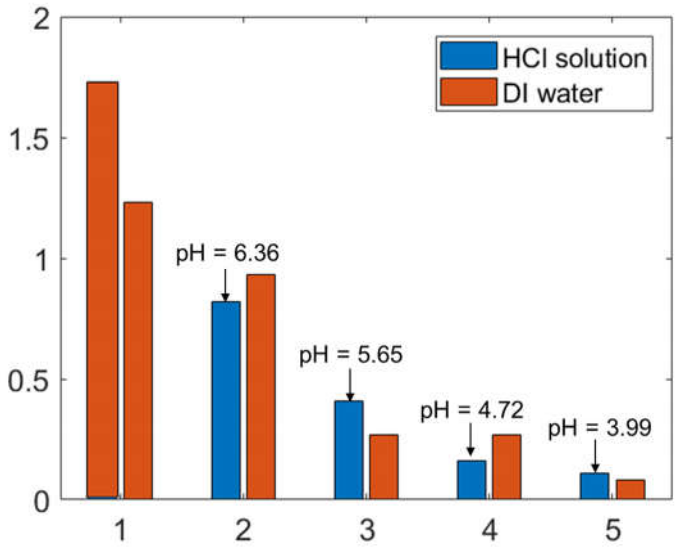

Figure. 3.5 Evaporation flux as function of fluid pH (nanopore diameter: 101±5 nm), after every HCl solution, the device was rinsed by water for 2 mins, then the DI water was used to do control experiment.

3.3 Summary and future work

In the Chapter 3, the effects of porosity and contaminant on kinetic-limited evaporation is investigated. Using the hybrid nanochannel-nanopore device, we measured the kinetic-limited evaporation rates from 3x3 nanopore arrays with different interval distances ranging from 200 nm to 1 μm. Our results showed that that the effects of porosity on kinetic-limited evaporation flux is negligible. We also done evaporation experiment using HCl as working fluid to study its effect on kinetic-limited evaporation flux. After series of experiment and SEM, it was believed that not the HCl in fluid but other contaminants in water can significantly reduce the kinetic-limited evaporation flux in nanopores and the contaminant effect becomes much more obvious in smaller nanopore due to contaminant-accumulation-induced pore blockage.

In the future, to further understand the effects of porosity, we should continuously reduce the interval distance between each single nanopore and make the distance even smaller than the feature size of nanopore diameter. And also, if we really want to investigate the correlation between HCl and kinetic-limited evaporation, to avoid the effect of other contaminant, for every HCl solution at certain concentration, we have to prepare a hybrid device and make sure the nanopore diameter of each device is similar

BIBLIOGRAPHY

Alkhudhiri, A., Darwish, N., & Hilal, N.. (2012). Membrane distillation: a comprehensive review. *Desalination,* 287, 2-18.

Bowers, M. B., & Mudawar, I. (1994). Two-phase electronic cooling using mini-channel and micro-channel heat sinks: Part 2—Flow rate and pressure drop constraints. *Journal of Electronic Packaging,* 116(4), 298-305.

Buckley, T. N., John, G. P., Scoffoni, C., & Sack, L. (2017). The Sites of Evaporation within Leaves. *Plant Physiology,* 173(3), 1763-1782. doi: 10.1104/pp.16.01605

Dai, X., Famouri, M., Abdulagatov, A. I., Yang, R., Lee, Y., George, S. M., & Li, C. (2013). Capillary evaporation on micromembrane-enhanced microchannel wicks with atomic layer deposited silica. *Applied Physics Letters,* 103(15), 151602. doi: 10.1063/1.4824439

Dai, X., Huang, X., Yang, F., Li, X., Sightler, J., Yang, Y., & Li, C.. (2013). Enhanced nucleate boiling on horizontal hydrophobic-hydrophilic carbon nanotube coatings. *Applied Physics Letters,* 102(16), 161605.

Dai, X., Yang, F., Yang, R., Lee, Y., & Li, C.. (2013). Micromembrane-enhanced capillary evaporation. *International Journal of Heat and Mass Transfer,* 64, 1101-1108.

Drisdell, W. S., Saykally, Richard J, & Cohen, Ronald C. (2010). Effect of surface active ions on the rate of water evaporation. *The Journal of Physical Chemistry C,* 114(27), 11880-11885.

Fang, J., Liu, Q., Zhang, W., Gu, J., Su, Y., Su, H., . . . Zhang, Di. (2017). Ag/diatomite for highly efficient solar vapor generation under one-sun irradiation. *Journal of Materials Chemistry A,* 5(34), 17817-17821.

Ghasemi, H., Ni, G., Marconnet, A. M., Loomis, J., Yerci, S., Miljkovic, N., & Chen, G. (2014). Solar steam generation by heat localization. *Nature Communications,* 5, 4449. doi: 10.1038/ncomms5449

Hertz. H. (1882). On the evaporation of liquids, especially mercury. In vacuo. *Annalen der Physik und Chemie.* Series 3, 17, 178(93).

Khayet, Mohamed. (2011). Membranes and theoretical modeling of membrane distillation: a review. *Advances in Colloid and Interface Science*, 164(1-2), 56-88.

Knudsen, Martin. (1950). *The kinetic theory of gases: Some modern aspects*. 3rd edition. London, Methuen; New York, Wiley.

Lee, Jongho, & Karnik, Rohit. (2010). Desalination of water by vapor-phase transport through hydrophobic nanopores. *Journal of Applied Physics,* 108(4), 044315.

Li, Y. (2017). Micro/nano structured phase change systems for thermal management applications. *PhD disstertion,* Boston University.

Lu, Z., Narayanan, S., & Wang, E. N. (2015). Modeling of Evaporation from Nanopores with Nonequilibrium and Nonlocal Effects. *Langmuir,* 31(36), 9817-9824. doi: 10.1021/acs.langmuir.5b01700

Lu, Z., Wilke, K. L., Preston, D. J., Kinefuchi, I., Chang-Davidson, E., & Wang, E. N. (2017). An Ultrathin Nanoporous Membrane Evaporator. *Nano Letters,* 17(10), 6217-6220. doi: 10.1021/acs.nanolett.7b02889

Lu, Z., Salamon, T. R, Narayanan, S., Bagnall, K. R., Hanks, Daniel F., Antao, Dion S,…Wang, E. N. (2016). Design and modeling of membrane-based evaporative cooling devices for thermal management of high heat fluxes. *IEEE Transactions on Components, Packaging and Manufacturing Technology,* 6(7), 1056-1065.

Marek, R, & Straub, J. (2001). Analysis of the evaporation coefficient and the condensation coefficient of water. *International Journal of Heat and Mass Transfer,* 44(1), 39-53.

Narayanan, S., Fedorov, A. G., & Joshi, Y. K. (2011). Interfacial transport of evaporating water confined in nanopores. *Langmuir,* 27(17), 10666-10676. doi: 10.1021/la201807a

Narayanan, S., Fedorov, A. G., & Joshi, Y. K. (2013). Heat and mass transfer during evaporation of thin liquid films confined by nanoporous membranes subjected to air jet impingement. *International Journal of Heat and Mass Transfer,* 58(1-2), 300-311. doi: 10.1016/j.ijheatmasstransfer.2012.11.015

Otten, Dale E, Shaffer, Patrick R, Geissler, Phillip L, & Saykally, Richard J. (2012). Elucidating the mechanism of selective ion adsorption to the liquid water surface. *Proceedings of the National Academy of Sciences of the Unites States of America,* 109(3), 701-705.

Pati, Sukumar, Som, SK, & Chakraborty, Suman. (2013). Combined influences of electrostatic component of disjoining pressure and interfacial slip on thin film evaporation in nanopores. *International Journal of Heat and Mass Transfer,* 64, 304-312.

Persad, Aaron H, & Ward, Charles A. (2016). Expressions for the evaporation and condensation coefficients in the Hertz-Knudsen relation. *Chemical Reviews,* 116(14), 7727-7767.

Plawsky, J. L., Fedorov, A. G., Garimella, S. V., Ma, H. B., Maroo, S. C., Chen, L., & Nam, Y. (2014). Nano- and Microstructures for Thin-Film Evaporation—A Review. *Nanoscale and Microscale Thermophysical Engineering,* 18(3), 251-269. doi: 10.1080/15567265.2013.878419

Rand, Richard H. (1983). Fluid mechanics of green plants. *Annual Review of Fluid Mechanics,* 15(1), 29-45.

Rizzuto, A. M., Cheng, E. S., Lam, R. K., & Saykally, R. J. (2017). Surprising Effects of Hydrochloric Acid on the Water Evaporation Coefficient Observed by Raman Thermometry. *The Journal of Physical Chemistry C,* 121(8), 4420-4425. doi: 10.1021/acs.jpcc.6b12851

Vafai, K., & Zhu, L.. (1999). Analysis of two-layered micro-channel heat sink concept in electronic cooling. *International Journal of Heat and Mass Transfer,* 42(12), 2287-2297.

Wang, Q., & Chen, R. (2018). Ultrahigh Flux Thin Film Boiling Heat Transfer Through Nanoporous Membranes. *Nano Letters.* doi: 10.1021/acs.nanolett.8b00648

Ward, CA, & Fang, G. (1999). Expression for predicting liquid evaporation flux: Statistical rate theory approach. *Physical Review E,* 59(1), 429.

Xiao, R., Maroo, S. C., & Wang, E.N. (2013). Negative pressures in nanoporous membranes for thin film evaporation. *Applied Physics Letters,* 102(12), 123103. doi: 10.1063/1.4798243

Yang, X., Yang, Y., Fu, L., Zou, M., Li, Z., Cao, A., & Yuan, Q.. (2018). An Ultrathin Flexible 2D Membrane Based on Single-Walled Nanotube-MoS2 Hybrid Film for High-Performance Solar Steam Generation. *Advanced Functional Materials,* 28(3), 1704505. doi: 10.1002/adfm.201704505

CURRICULUM VITAE